Meshless methods for 'gas - evaporating droplet' flow modelling

Oyuna Rybdylova, Sergei S Sazhin

The Sir Harry Ricardo Laboratories, Advanced Engineering Centre,
School of Computing, Engineering and Mathematics, University of Brighton, UK

E-mail: O.Rybdylova@brighton.ac.uk; S.Sazhin@brighton.ac.uk

Abstract. The main ideas of simulation of two-phase flows, based on a combination of the conventional Lagrangian or fully Lagrangian (Osiptsov) approaches for the dispersed phase and the mesh-free vortex and thermal-blob methods for the carrier phase, are summarised. In the approach based on a combination of the fully Lagrangian approach for the dispersed phase and the vortex blob methods for the carrier phase the problem of calculation of all parameters in both phases (including particle concentration) is reduced to the solution of a high-order system of ordinary differential equations, describing transient processes in both carrier and dispersed phases. It contrast to this approach, in the approach based on a combination of the conventional Lagrangian approaches for the dispersed phase and the vortex and thermal-blob methods for the carrier phase the non-isothermal effects in the two-phase flow were taken into account. The one-way coupled, two-fluid approach was used in the analysis. The gas velocity field was restored using the Biot-Savart integral. Both these approaches were applied to modelling of two processes: the time evolution of a two-phase Lamb vortex and the development of an impulse two-phase jet. Various flow patterns were obtained in the calculations, depending on the initial droplet size.

1. Introduction

Two-phase flows are widely observed in engineering and environmental conditions (e.g. [1]). In such flows, the admixture sometimes forms high concentration regions with complex structures [1]. The Eulerian approaches cannot describe such regions with reasonable accuracy, since these approaches are based on the assumption of single-valued fields of the particle/droplet concentration and velocities. As demonstrated in [2], the only approach capable of calculating the droplet concentration field, without using excessive computer power, is the one suggested by Osiptsov [3]. The latter approach is commonly known as the Osiptsov method or approach.

Various meshless methods for the carrier phase flows have been developed and have proved to be efficient tools for investigating complex single-phase flows both with primitive and vorticity-velocity variables (e.g. [4]). Lebedeva et al. [5] developed and tested a method combining the viscous-vortex method for the carrier phase and Osiptsov's approach [3] for particles/droplets. This approach combined the advantages of both the viscous-vortex and Osiptsov methods.

The approaches mentioned above were focused on hydrodynamic aspects of particle-laden flows. However, in many engineering applications, including automotive applications [6], the effects of heat and mass transfer are significant. In [7] some aspects of the approach described in [5] were generalised to take into account some of these effects. The phase transition on the

droplet surface was described using a simple model based on the assumption that the heat flux reaching the droplet is spent on its evaporation (cf. a similar assumption used for qualitative engineering analysis of droplet evaporation in multiphase flows ([6, 8]).

The aim of this paper is to present a summary of the models developed and used in the previous papers [5, 7] (Section 2) and the main results obtained (Section 3). The main results of this paper are summarised in Section 4. The publication of this mini-review can be justified by the fact that the original papers were published in engineering journals which are almost unknown to the mathematical community. At the same time, these papers are focused primarily on the description of new mathematical tools and their engineering applications, which are expected to be relevant to mathematical research in this field.

2. Models

In what follows, the main ideas of the models developed and used for 2D plane flows (Cartesian coordinates) in [5, 7] are briefly summarised.

2.1. Fully Lagrangian (Osiptsov) method

In the fully Lagrangian (Osiptsov) approach [3] the dispersed phase number density is inferred from the solutions to the following system of ordinary differential equations along chosen droplet trajectories:

$$n_s \left| J \right| = n_{s0} \tag{1}$$

$$\frac{\partial \mathbf{x}_s}{\partial t} = \mathbf{v}_s, \quad \frac{\partial \mathbf{v}_s}{\partial t} = \beta(\mathbf{v} - \mathbf{v}_s)\chi_d + \frac{1}{\mathrm{Fr}^2}\mathbf{e}_g, \tag{2}$$

$$\frac{\partial J_{ij}}{\partial t} = q_{ij}, \tag{3}$$

$$\frac{\partial q_{ij}}{\partial t} = \beta\left(\frac{\partial v_i}{\partial x}J_{xj} + \frac{\partial v_i}{\partial y}J_{yj} - q_{ij}\right)\chi_d + \beta\left(v_i - v_{si}\right)\frac{\partial \chi_d}{\partial x_{j0}}, \tag{4}$$

$$\frac{\partial \chi_d}{\partial x_{j0}} = \frac{1}{9}\frac{\mathrm{Re}_{s0}}{\mathrm{Re}_s^{1/3}}\frac{1}{\left|\mathbf{v} - \mathbf{v}_s\right|}\left(\left(u - u_s\right)\left(\frac{\partial u}{\partial x}J_{xj} + \frac{\partial u}{\partial y}J_{yj} - q_{xj}\right) + \right.$$
$$\left. + \left(v - v_s\right)\left(\frac{\partial v}{\partial x}J_{xj} + \frac{\partial v}{\partial y}J_{yj} - q_{yj}\right)\right),$$

where

$$J_{ij} = \frac{\partial x_i}{\partial x_{j0}}, \quad q_{ij} = \frac{\partial v_{si}}{\partial x_{j0}}, \; \chi_d = 1 + \mathrm{Re}_s^{2/3}/6,$$

$$\beta = \frac{6\pi\sigma\mu R_0^2}{m\Gamma_0}, \quad \mathrm{Fr} = \frac{\Gamma_0}{R_0\sqrt{gR_0}}, \quad \mathrm{Re}_s = \mathrm{Re}_{s0}\left|\mathbf{v} - \mathbf{v}_s\right|, \quad \mathrm{Re}_{s0} = \frac{2\sigma\Gamma_0}{R_0\nu},$$

indices i and j take values of x or y in the Cartesian coordinate system; $\mathbf{e}_g$ is the unit vector along the direction of the gravity force; x_{s0}, y_{s0} are the Lagrangian variables (the coordinates of initial particle positions); J is the Jacobian of the transformation from the Eulerian to the Lagrangian coordinates.

Equation (1) is the continuity equation rewritten in the Lagrangian variables. Equations (2) are momentum balance equations along chosen particle trajectories. Equations (3) and (4) are additional equations to calculate the Jacobian components; they are derived from Equations (2) by differentiation with respect to x_{s0} and y_{s0}. These equations are solved subject to standard initial conditions.

These equations were presented for plane geometry. Their generalisation to cylindrical geometry is straightforward (see [3] for the details).

2.2. Viscous-vortex and thermal-blobs

In the viscous-vortex and thermal-blob methods the dimensionless carrier phase equations are written in the form [7]:

$$\frac{\partial \omega}{\partial t} + \operatorname{div}(\omega \mathbf{v}) = \frac{1}{\mathrm{Re}} \Delta \omega, \tag{5}$$

$$\frac{\partial T}{\partial t} + \operatorname{div}(T \mathbf{v}) = \frac{\gamma}{\mathrm{Re}\,\mathrm{Pr}} \Delta T, \tag{6}$$

where $\omega = \nabla \times \mathbf{v}$ is the vorticity; $\mathrm{Re} = \rho L U / \mu$ and $\gamma = c_p / c_v$ are the Reynolds number and the specific heat ratio; ρ, μ and U are density, dynamic viscosity and velocity of the carrier phase. The following non-dimensional parameters were used:

$$\mathbf{r}(\mathbf{r}_s) = \frac{\mathbf{r}^*(\mathbf{r}_s^*)}{L},\ \mathbf{v}(\mathbf{v}_s) = \frac{\mathbf{v}^*(\mathbf{v}_s^*)}{U}, T(T_s) = \frac{T_\infty - T^*(T_s^*)}{T_\infty - T_{ref}},\ \sigma = \frac{\sigma^*}{\sigma_{ref}},$$

$$\mathbf{r} = (x, y),\ \mathbf{r}_s = (x_s, y_s),\ \mathbf{v} = (u, v),\ \mathbf{v}_s = (u_s, v_s),$$

where L and U are the length and velocity scales of the problem; T_{ref} and T_∞ are the gas dimensional reference temperature (e.g. jet temperature at the inlet) and the temperature in the far field, respectively, σ_{ref} is the droplet radius scale (e.g. initial droplet radius in the case of initially monodisperse droplets); the so-defined dimensionless temperature takes values between 0 and 1, with 0 corresponding to the temperature in the far field.

Equation (5) is the vorticity transport equation which follows from the Navier-Stokes equations for an incompressible fluid. Equation (6) is the transient heat conduction equation.

Introducing the vortex and thermal diffusion velocities, $\mathbf{v}_{dv}$ and $\mathbf{v}_{dT}$, Equations (5) and (6) can be presented in the divergence forms:

$$\frac{\partial \omega}{\partial t} + \operatorname{div}(\omega(\mathbf{v} + \mathbf{v}_{dv})) = 0, \tag{7}$$

$$\frac{\partial T}{\partial t} + \operatorname{div}(T(\mathbf{v} + \mathbf{v}_{dT})) = 0, \tag{8}$$

where

$$\mathbf{v}_{dv} = -\frac{1}{\mathrm{Re}} \frac{\nabla \omega}{\omega},\ \mathbf{v}_{dT} = -\frac{\gamma}{\mathrm{Re}\,\mathrm{Pr}} \frac{\nabla T}{T}.$$

This allows tracking of viscous-vortex and thermal-blobs moving with velocities $v + v_{dv}$ and $v + v_{dT}$, respectively, by solving ODEs subject to corresponding initial conditions. Then vorticity and temperature fields are calculated using Equations (7) and (8).

For calculation of vorticity, the domain with a non-zero vorticity is discretised into N elements, with the area of the i-th element equal to Δ_{vi}:

$$\omega(\mathbf{r}, t) \approx \sum_{i=1}^{N} \Gamma_i \zeta_{\varepsilon_i}(\mathbf{r} - \mathbf{r}_{vi}(t)), \tag{9}$$

$$\Gamma_i \approx \omega_0(\mathbf{r}_{vi}(t_0))\, \Delta_{vi} = \mathrm{const}, \tag{10}$$

where $\zeta_{\varepsilon_i}(\mathbf{r})$ are the so-called cut-off functions. The elements of discretisation are called blobs.

Similarly, the equations for M thermal blobs take the form:

$$T(\mathbf{r}, t) \approx \sum_{i=1}^{M} \Theta_i \zeta_{\varepsilon_i}(\mathbf{r} - \mathbf{r}_{Ti}(t)), \tag{11}$$

$$\Theta_i = T_0(\mathbf{r}_{Ti}(t_0))\, \Delta_{Ti} = \mathrm{const}, \tag{12}$$

where Θ_i and $\mathbf{r}_{Ti}$ are the strength and position of the i-th thermal blob.

Once the vorticity field is calculated, then the velocity field can be restored using the Biot-Savart integral.

3. Results

In this section, some results obtained using a combined fully Lagrangian and viscous-vortex blob approach (originally reported in [5]) and a combined conventional Lagrangian, viscous-vortex blob and thermal-blob approach (originally reported in [7]) are briefly summarised.

3.1. A combined fully Lagrangian and viscous-vortex blob approach

The approach based on a combination of the fully Lagrangian method for the dispersed phase and the mesh-free viscous-vortex blob method for the carrier phase was suggested and tested in [5]. In this section the main findings reported in the latter paper are briefly summarised.

This approach was applied to modelling of two processes: the time evolution of a two-phase Lamb vortex and the development of an impulse two-phase jet. These examples involve the formation of local zones of particle accumulation and regions of multiple intersection of particle trajectories. These features of the flow cannot be simulated using the conventional Eulerian and Lagrangian methods described in the literature.

3.1.1. Isothermal Lamb vortex flow The distribution of the vorticity and the azimuthal velocity of the Lamb vortex flow are described by the following equations (r is the distance from the vortex centre):

$$\omega = \frac{\mathrm{Re}}{4\pi t}\exp\left(-\mathrm{Re}\frac{r^2}{4t}\right), \tag{13}$$

$$v_\varphi = \frac{1}{4\pi}\left[1-\exp\left(-\mathrm{Re}\frac{r^2}{4t}\right)\right], \tag{14}$$

where $\mathrm{Re} = \Gamma_0/\nu_g$, Γ_0 and ν_g are the circulation of the Lamb vortex and gas kinematic viscosity, respectively. These expressions are presented in dimensionless form, where the scales for length, velocity, time, and vorticity are taken equal to the particle velocity relaxation length $\ell_\tau = (m\Gamma_0/(6\pi\sigma\mu_g))^{1/2}$, $U = \Gamma_0/\ell_\tau$, $T = \ell_\tau^2/\Gamma_0$ and $W = \Gamma_0/\ell_\tau^2$, respectively. These expressions were used in [5] for verification of the numerical algorithm for calculation of vorticity and velocity for the carrier phase.

It was shown in [5] that the vorticity value found when the number of vortex blobs is of the order of one thousand, and the value found from the exact solution are very close. This verifies the method of calculating the carrier phase parameters, described earlier.

The dynamics of the dispersed phase are described in [5] by the following system of equations:

$$\frac{\partial \mathbf{v}_s(t,\mathbf{r}_{s0})}{\partial t} = a\left(\mathbf{v}-\mathbf{v}_s\right) + b\frac{\mathrm{d}\mathbf{v}}{\mathrm{d}t} + c\mathbf{e}_g, \tag{15}$$

$$\frac{\partial \vartheta_{pq}}{\partial t} = a\left(D_q\left[(\mathbf{v})\right]-\vartheta_{pq}\right) + bD_q\left[\frac{\mathrm{d}(\mathbf{v})_p}{\mathrm{d}t}\right], \tag{16}$$

where,

$$D_q = J_{1q}\frac{\partial}{\partial x} + J_{2q}\frac{\partial}{\partial y}$$

$$a = \frac{2}{2+\eta},\quad b = \frac{3\eta}{2+\eta},\quad c = \frac{2-2\eta}{(2+\eta)\mathrm{Fr}^2},\quad \eta = \frac{\rho_f}{\rho_s},\quad \mathrm{Fr}^2 = \frac{U^2}{gL},$$

ρ_s is the density of the particles and $\mathbf{e}_g$ is a unit vector in the direction of the gravity force (as in the previous formulae). Normalising the particle number density by its initial value n_0 (assumed to be constant over the whole region occupied by the particles), we can write:

$$n_{sj}\left|J_j\right| = 1. \tag{17}$$

These equations were solved subject to the following initial conditions:

$$t = 1: \quad \mathbf{r}_{sj} = \mathbf{r}_{0j}, \quad \mathbf{v}_{sj} = 0, \quad J_{pq,\,j} = 1 \; (p \neq q), \quad \vartheta_{pq,j} = 0.$$

The number of particle trajectories was taken equal to the number of blobs: $M = N$.

The authors of [5] showed some examples of the calculations for different values of parameters η and Fr. They illustrated the time evolution of particle number density for the case when $\rho_s \gg \rho_g$ (i.e. $\eta \to 0$) under the assumption that only the effect of the Stokes drag force needs to be taken into account. In this case, the particles, initially uniformly distributed in space, eventually left the high-vorticity region and formed a ring-shaped particle accumulation zone. The ring radius increased with time and sharp concentration gradients developed on the edge of the particle accumulation zone. It was shown that, in the presence of gravity, the particle accumulation region was deformed and removed from the vortex centre. The particle concentration gradient near the boundary of the particle cloud in this case increased with time.

When the density of particles was less than that of the carrier phase, $\rho_s < \rho_g$ (i.e. $\eta > 1$), the flow pattern became rather different from the one described above. In this case, the contribution of the added mass force became predominant. This force led to particle penetration into the high-vorticity region. The centrifugal force, however, resulted in their displacement away from the vortex centre. As a result, the shape of the particle cloud changed non-monotonically with time. The formation of annular zones of particle accumulation in the high-vorticity region was demonstrated. The effect of gravity on these particles was shown to lead to the formation of a particle cloud, with narrow zones of particle inhomogeneity. This cloud was shown to leave the centre of the vortex, significantly increasing in size with time. In this flow, multiple intersections of particle trajectories were observed. To represent the instantaneous patterns of the total particle number density in the regions of multi-valued particle velocities (folds) an additional recalculation procedure was used. This procedure included checking the sign of Jacobian J and the comparison of the values of particle velocities for particle trajectories when these trajectories became very close. When the signs of J or the velocities of the neighbouring trajectories were different, the total particle density was calculated as the sum of different parts of the 'fold'.

3.1.2. Isothermal two-phase plane jet flow Apart from particle flows in a Lamb vortex, the authors of [5] considered an impulse plane two-phase jet, injected into a quiescent carrier phase during Δt. Only the Stokes drag was taken into account. The initial dimensional particle number density n_0 was assumed to be uniform. The particle number density in the mixture was normalised by this value. Three numbers of vortex blobs N were used in the initial calculations: 400, 1000 and 2000. It was shown that the predicted values of velocity for $N = 1000$ and $N = 2000$ were almost indistinguishable. This allowed the authors of [5] to use $N = 1000$ in all their calculations. The values of the maximal velocities were shown to decrease with time, as expected for the post-formation stage of the vortex pair development. The dependence of the predicted velocities on Re (Re = 50, Re = 100, Re = 1000) was shown to be weak at the initial stage of the process; it became more noticeable at a later stage. The carrier phase and vortex pair velocities increased with Re, which is consistent with the vortex pair theory.

Two initial conditions were considered. The first one corresponded to the case when a single-phase jet was injected into a quiescent two-phase mixture with uniform particle concentration, and the second one referred to the injection of a two-phase jet into the pure carrier phase. For the first case, it was shown that particles accumulated near the edges of the vortex pair. For the second case, the deformation of Lagrangian dispersed phase volumes in the flow was shown to be rather complex. In this case, the distribution of the particle concentration could not be correctly calculated on the basis of conventional approaches.

3.2. A combined Lagrangian, viscous-vortex blob and thermal-blob approach
The approach based on a combination of the conventional Lagrangian method for the dispersed phase and viscous-vortex and thermal-blob methods for the carrier phase was suggested and tested in [7]. In this section the main findings reported in the latter paper are briefly summarised.

As in the case considered in the previous section, this approach was applied to modelling of two processes: the time evolution of a two-phase Lamb vortex and the development of an impulse two-phase jet. In contrast to the previous section, the effects of droplet heating and evaporation were taken into account although based on a rather simplistic model. Hence, the analysis of that paper was focused specifically on droplets rather than on particles (which would have included both solid particles and droplets).

It was assumed that the heat flux is directed towards the droplets. Only evaporation was considered and not droplet heating. Given these simplifications, the evaporation rate is controlled by the heat reaching the surface of the droplet:

$$\dot{m} = \frac{q_s}{H}. \tag{18}$$

The corresponding dimensionless equation can be written in the Lagrangian form:

$$\frac{d\sigma^2}{dt} = \delta\left(T - T_s\right)\Psi_h, \tag{19}$$

where

$$\delta = \frac{8\pi}{3}\frac{\sigma_{ref} L\lambda^*\left(T_\infty - T_{ref}\right)}{m_{ref} UH}, \Psi_h = 1 + 0.3\mathrm{Pr}^{1/3}\mathrm{Re}_s^{1/2}, \;\; \mathrm{Pr} = c_p\mu^*/\lambda^*,$$

δ is the droplet evaporation parameter; m_{ref} is the mass of a droplet of radius σ_{ref}, H is the latent heat of evaporation, λ^* is the dimensional gas thermal conductivity.

3.2.1. Non-isothermal Lamb vortex flow As in the previous section, the Lamb vortex was described by Equations (13) and (14). The initialisation of the viscous-vortex blobs was the same as described in the previous section, except that the blobs were placed on concentric circumferences, with the radii increasing with a fixed step $\Delta r = 0.025$ (rather than the step decreasing towards the vortex centre). This led to a series of rings, with the blobs distributed uniformly in each ring. The strength of the blobs was calculated as the difference in the circulations around the outer and inner radii at $t = t_0$ divided by the number of blobs in the ring. Since Solution (13)-(14) has a singularity at $t = 0$, the initial time instant was taken as $t_0 = 1$. Increasing the number of blobs in the calculations, it was found that a satisfactory accuracy could be achieved with 863 viscous-vortex blobs, and a core size $\varepsilon = c_\varepsilon\sqrt{h}$, where h is the width of the corresponding ring, $c_\varepsilon = 0.7$.

For this number of blobs the algorithm gave satisfactory results not only for the velocity field but also for the derivatives of the velocity. The numerical code was verified by comparison of the predicted results with those inferred from Solution (13)-(14). The closeness of these results shows that the numerical code can be expected to be reliable and can be used for the analysis of other flows.

In the next step, the thermal part of the algorithm was verified. This verification was based on the observation that Equation (5) is equivalent to Equation (6), if $\gamma = \mathrm{Pr}$. Hence, an exact solution for the dimensionless temperature field evolution, corresponding to the diffusion of the localised temperature non-uniformity in the Lamb vortex field, can be described as:

$$T = \frac{\mathrm{Re}}{4\pi t}\exp\left(-\mathrm{Re}\frac{\mathbf{r}^2}{4t}\right) \tag{20}$$

Expression (20) was used to verify the calculations of the temperature field distribution. The initial location of thermal blobs was the same as that of the viscous-vortex blobs. For $\mathrm{Re} = 100$, the initial temperature distribution was set as $T = 25/\pi \exp\left(-25r^2\right), t_0 = 1$. The strength of each thermal blob was the temperature at the blob centre, multiplied by the blob area (the area of a ring divided by the number of blobs in the ring). As in the case of the vorticity field, the results for the temperature were shown not to depend on the number of thermal blobs when this number exceeded 863. The latter number of thermal blobs was used in the analysis of [7].

At the next stage, the droplet parameters were calculated. The droplet evaporation was calculated for $\mathrm{Re} = 100$, $\mathrm{Pr} = 0.8$, $\gamma = 1.33$, $\mathrm{Re}_{s0} = 0$, $\delta = -0.1$, where γ is the specific heat ratio. The initial dimensionless temperature distribution was set as $T = \exp\left(-r^2/0.04\right)$, which implies that $0 < T \leq 1$. The fields of the droplet parameters were presented as functions of the distance to the axis of symmetry. The initial conditions for the dispersed phase were the following:

$$t = t_0 : \ \mathbf{r}_s = \mathbf{r}_0, \ \mathbf{v}_s\left(\mathbf{r}_s\right) = \mathbf{v}\left(\mathbf{r}_s\right), T_s\left(x, y\right) = 0, \ \sigma = 1.$$

Inertial droplets were shown to have a tendency to move away from the centre of the vortex. The droplets initially positioned closer to the vortex centre had higher initial velocities and they overtook the droplets initially located at the periphery. The trajectory intersections resulted in the formation of a multivalued field of droplet parameters. The central region of the flow corresponded to the highest difference in the temperatures between the carrier and the dispersed phases, which led to the highest evaporation rates. The effect of the evaporation process on the drag force coefficient was not explicitly taken into account, but this drag force reduced, as droplet radii decreased. As droplets evaporated, their inertia decreased; the droplet velocities were closer to those of the carrier phase in the case of evaporating droplets, compared with the case of non-evaporating droplets.

3.2.2. Non-isothermal plane two-phase jet flow In what follows, the results of application of the same model as described in the previous section to the analysis of the injection of a cold, two-phase jet into a hot, quiescent gas are described. This study was focused on the formation and dynamics of a two-phase vortex pair.

The injection of a water spray with $L = 0.01$ m (nozzle width), $U = 1.5$ m/s, $T^*_\infty - T^*_{ref} = 50$ K (superscript * indicates dimensional temperatures) was considered. A Cartesian coordinate system with the x-axis directed along the jet axis of symmetry, and the origin at the inlet of the jet was used.

In the calculations, the initial dimensionless vorticity distribution corresponded to a smooth step-like velocity profile in the form:

$$u_0 = \frac{1}{1 + \exp\left(-100\left(y + 0.4\right)\right)} + \frac{1}{1 + \exp\left(100\left(y - 0.4\right)\right)} - 1, \quad v_0 = 0. \tag{21}$$

The initial dimensionless temperature distribution was taken as $T_0\left(x, y\right) = u_0\left(x, y\right)$. The initial conditions for the dispersed phase were assumed to be the following:

$$t = t_0 : \ \mathbf{r}_s = \mathbf{r}_0, \ \mathbf{v}_s = \left(u_{s0}, v_{s0}\right) = \left(0.8, 0\right), \ \ T_s\left(x, y\right) = 1, \ \sigma = 1.$$

The vorticity inferred from the velocity distribution described by System (21) was zero in most of the domain, including the axis $y = 0$, but excluding the two small regions at negative and positive y. This allowed the authors of [7] to initially position the viscous blobs in two rectangles $[-4; 0] \times [0.24; 0.56]$ and $[-4; 0] \times [-0.56; -0.24]$. The thermal blobs were located initially in the rectangle $[-4; 0] \times [-0.5; 0.5]$. The domain geometry ($D/L = 4$) corresponded to the vortex pair 'formation number'. The droplets occupied the rectangle $[-4; 0] \times [-0.4; 0.4]$. At the initial time instant, the regions on both sides of the injected liquid column were free of droplets, and

the droplet velocities were 20% lower than those of the carrier phase. At the initial instant of time, all blobs and droplets were distributed uniformly. The strength of a blob was calculated as the product of the corresponding value of the parameter (vorticity or temperature) and the blob area. The variable core size for each blob was calculated as $\varepsilon_i = c_\varepsilon \min\limits_{j=\overline{1,N}} \left(\sqrt{|\mathbf{r}_{vj} - \mathbf{r}_{vi}|}\right)$ for viscous-vortex blobs, and $\varepsilon_i = c_\varepsilon \min\limits_{j=\overline{1,M}} \left(\sqrt{|\mathbf{r}_{Tj} - \mathbf{r}_{Ti}|}\right)$, for thermal blobs, where $c_\varepsilon = 1.01$.

After the injection, the viscous-vortex blobs concentrated in two spirals, swirled in the opposite directions and propagating into the quiescent gas. The initial locations and velocities of thermal blobs differed from those of viscous-vortex blobs and they fill a region different from the one occupied by the viscous-vortex blobs.

The numerical results for the carrier phase velocity fields were compared with the results predicted by the asymptotic analytical solution to the problem of the diffusion of a vortex pair, according to which the 'centres' of the vorticity regions travel with velocity:

$$V_{VC}\left(\frac{t^*\Gamma_{\text{ini}}}{l_0^2}\right) = \frac{\Gamma_{\text{ini}}}{4\pi l_0}\left[1 - 8.736\left(\frac{t^*\nu}{l_0^2}\right)^2 + 1.845\left(\frac{t^*\nu}{l_0^2}\right)^3\right]. \tag{22}$$

The asymptotic solution (22) is valid for high Reynolds numbers $\text{Re}_a = \Gamma_{\text{ini}}/\nu >> 1$. In this equation, Γ_{ini} is the intensity of each of the vortices at the initial time instant, and $\pm l_0$ are the initial ordinates of the vortices. Since the vortex pair was symmetric, only the top vortex position was calculated using the formula:

$$\Gamma_{\text{top}} = \sum_{i:\ y_{vi}>0} \Gamma_i, \quad \mathbf{r}_{VC} = \frac{1}{\Gamma_{\text{top}}} \sum_{i:\ y_{vi}>0} \mathbf{r}_{vi}\Gamma_i \tag{23}$$

The reference values for the vortex centre position and velocity were taken at $t = 4$. For Solution (22) the initial time instant was taken equal to $t_0 = 2.6$. The calculations were performed for 10000 viscous-vortex blobs, 10000 thermal blobs, and 1681 droplets.

The 'thermal centres' were calculated using the formula

$$\Theta_{\text{top}} = \sum_{i:\ y_{vi}>0} \Theta_i, \quad \mathbf{r}_{TC} = \frac{1}{\Theta_{\text{top}}} \sum_{i:\ y_{vi}>0} \mathbf{r}_{Ti}\Theta_i.$$

Vortex centre dynamics predicted by the numerical simulation were compared with the prediction of the asymptotic solution (see (22)) for the cases of $\text{Re} = 100$ and $\text{Re} = 1000$. It was shown that the asymptotic solution ($\text{Re} \to \infty$) predicts slightly higher values than the numerical simulations; there was a better agreement between the results for the case of $\text{Re} = 1000$. In both cases the numerical results agreed satisfactorily with the predictions of the analytical solution at the initial times ($0 < t < 10$); at later times the discrepancy increased.

The cases of droplets with $\beta = 5.5$, $\beta = 0.21$, and $\beta = 0.05$ were considered. In Figs. 1-3, reproduced from [7], clouds of droplets at various time instants are presented. In the top parts of the figures, the highest level of shading corresponds to the largest droplets, and the lowest level to the smallest droplets. In the bottom parts of the figures, the highest level of shading corresponds to the largest phase velocity slips, and the lowest level to the smallest velocity difference. As one can see in these figures, after the injection, a vortex pair forms in the carrier

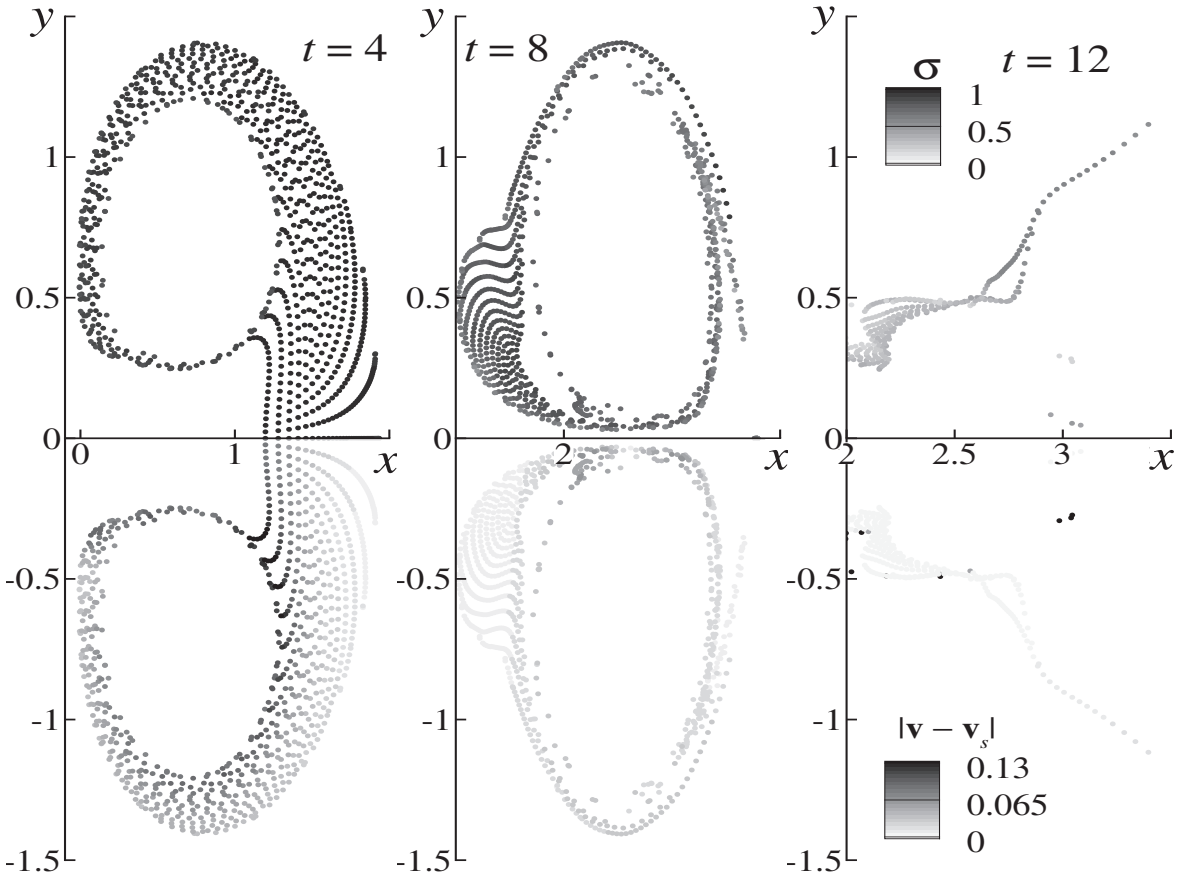

Figure 1. Droplet distributions, their sizes, and velocity slips at $t = 4$, $t = 8$ and $t = 12$; $\beta = 5.5$, $\delta = 0.14$. Reprinted from Ref. [7]. Copyright Elsevier (2016)

phase. The velocities of low-inertia particles ($\beta = 5.5$, see Fig. 1) are quicker to relax than the carrier phase velocities. Thus, the two-phase flow is characterised by better mixing; the droplets form ring-like structures and evaporate more quickly when compared with the cases of larger droplets. At $t = 8$, smaller droplets are located closer to the jet axis, while larger droplets can be seen at the periphery.

The case $\beta = 0.21$ (see Fig. 2) corresponds to the widest two-phase jet among the cases considered. The velocities of the droplets, that were initially close to the inlet, decrease as they enter the quiescent gas; the droplets that enter the flow later can overtake the leading edge. The initially rectangular cloud of droplets is turned inside out after the injection, then it is deformed into a narrow band (see $t = 8$, $t = 12$). The droplets at the sides move more slowly and evaporate more rapidly than those at the centre. As the droplets at the front of the two-phase region evaporate and slow down, larger droplets move to the front edge ($t = 12$). At later times the cloud of droplets is divided into two groups, positioned along the jet axis. The droplet sizes vary within a 7% range.

In the case of droplets with greater inertia ($\beta = 0.05$, see Fig. 3), their sizes remain almost unchanged. The cloud of droplets deforms into a narrow band. The droplets evaporate at a greater rate at the front of the two-phase region. Hence, larger droplets stay at the rear of the droplet cloud. The two-phase region stays closer to the jet axis.

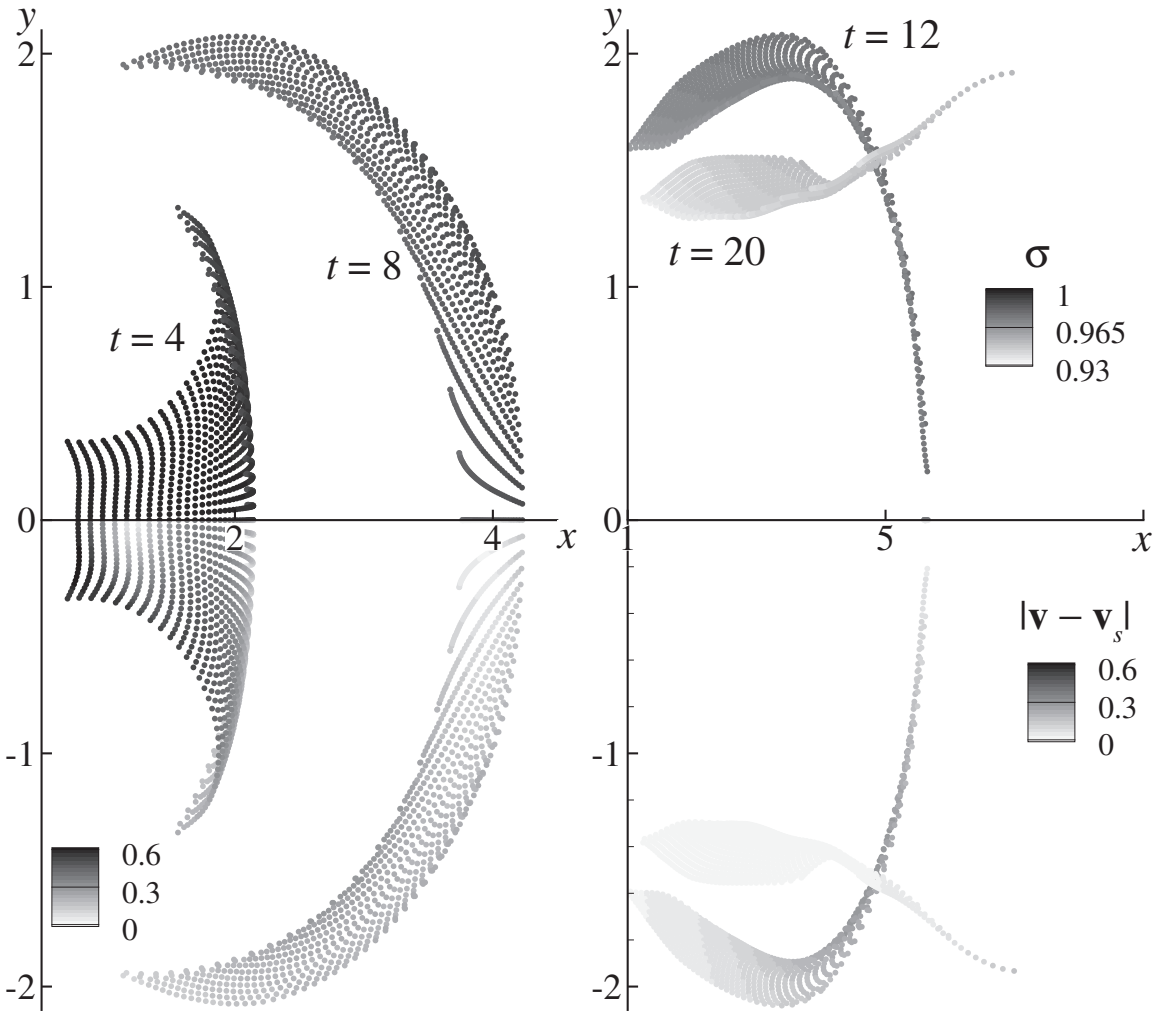

Figure 2. Droplet distributions, droplet diameters, and velocity slips at $t = 4$, $t = 8$, $t = 12$, and $t = 20$; $\beta = 0.21$, $\delta = 0.006$. Reprinted from Ref. [7]. Copyright Elsevier (2016)

4. Conclusions

New approaches to numerical simulation of two-phase flows suggested in [5, 7] have been discussed and summarised. In [5] an approach to numerical simulation of two-phase flows, based on a combination of the fully Lagrangian method for the dispersed phase and the mesh-free vortex blob method for the carrier phase, was suggested and tested. The one-way coupled, two-fluid approach was used in the analysis. The gas velocity field was restored using the Biot-Savart integral. In this case, the problem of calculation of all parameters in both phases (including particle concentration) is reduced to the solution of a high-order system of ordinary differential equations, describing transient processes in both carrier and dispersed phases. This allows one to study in detail local zones of particle accumulation in complex transient flows, including those with multiple intersections of particle trajectories and the formation of 'folds' in the concentration field of the dispersed phase.

This approach was applied to modelling of two processes: the time evolution of a two-phase Lamb vortex and the development of an impulse two-phase jet. These examples involve the

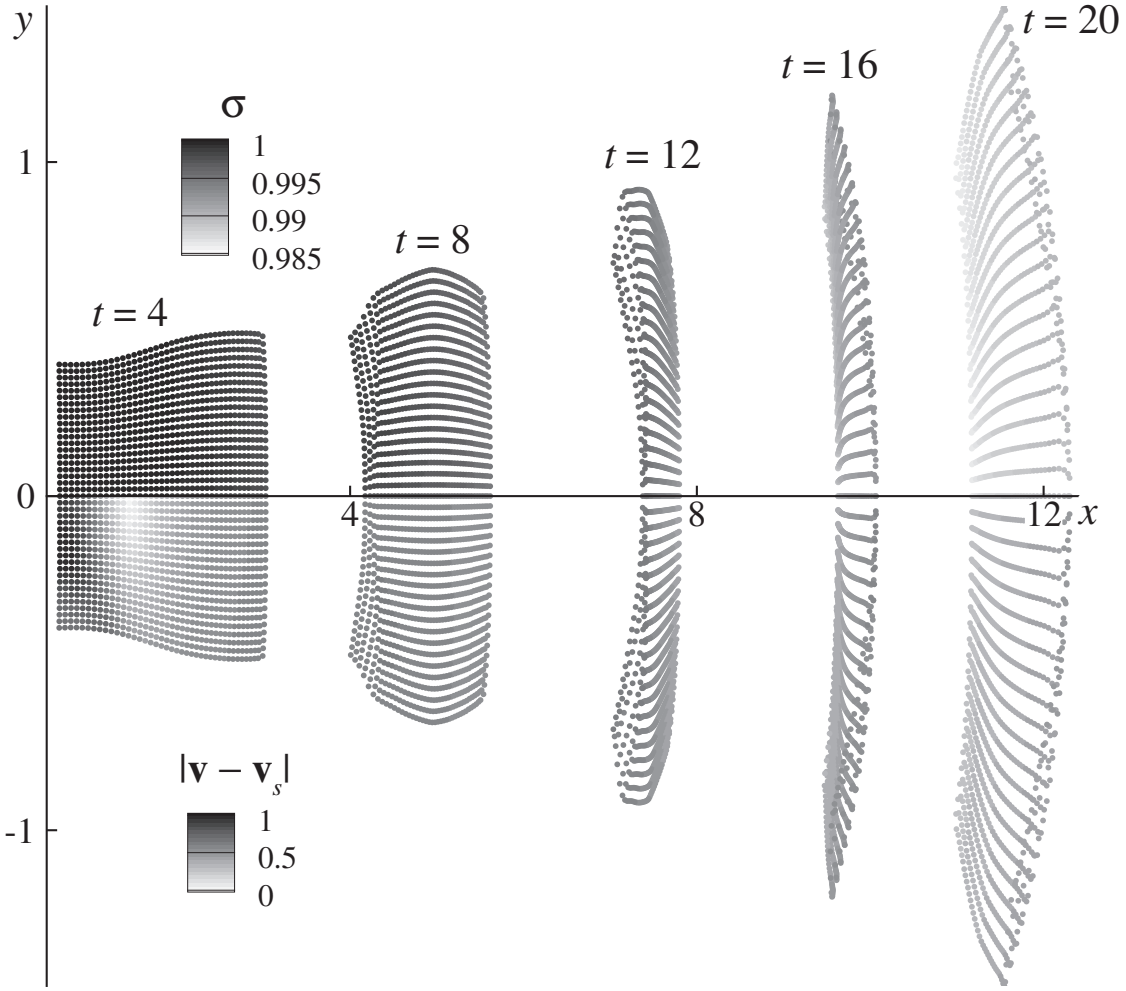

Figure 3. Droplet distributions, droplet diameters, and velocity slips at $t = 4$, $t = 8$, $t = 12$, $t = 16$, and $t = 20$; $\beta = 0.05$, $\delta = 0.0014$. Reprinted from Ref. [7]. Copyright Elsevier (2016)

formation of local zones of particle accumulation and regions of multiple intersection of particle trajectories. These features of the flow cannot be simulated using the conventional Eulerian and Lagrangian methods described in the literature.

In the approach described in [7] the results of the development of a method for modelling of 2D transient, non-isothermal, gas-droplet flows with phase transitions, based on a combination of the viscous-vortex and thermal-blob methods for the carrier phase with the Lagrangian approach for the dispersed phase, were presented. As in [5], the one-way coupled, two-fluid approach was used in the analysis and the gas velocity field was restored using the Biot-Savart integral. The numerical algorithm was verified against the analytical solution for a non-isothermal Lamb vortex and some asymptotic results known in the literature. The method was applied to modelling of an impulse two-phase cold jet injected into a quiescent hot gas, taking into account droplet evaporation. Various flow patterns were obtained in the calculations, depending on the initial droplet size: (i) low-inertia droplets, evaporating at a higher rate, formed ring-like structures and were accumulated only behind the vortex pair; (ii) large droplets moved closer to the jet

axis, with their sizes remaining almost unchanged; and (iii) intermediate-size droplets were accumulated in a curved band whose ends trail in the periphery behind the head of the cloud, with larger droplets being collected at the front of the two-phase region.

Acknowledgments
The authors are grateful to EPSRC (grants EP/K005758/1 and EP/M002608/1) for their financial support.

References

[1] Begg S, Kaplanski F, Sazhin S S, Hindle M, and Heikal M 2009 *International Journal of Engine Research* **10** (4) (2009) 195
[2] Healy D and Young J 2005 *Proceedings of the Royal Society of London A: Mathematical, Physical and Engineering Sciences* **461**(2059) 2197
[3] Osiptsov A N 2000 *Astrophys. Space Sci.* **274** 377
[4] Monaghan J 2012 *Annual Review of Fluid Mechanics* **44** 323
[5] Lebedeva N A, Osiptsov A N and Sazhin S S 2013 *Atomization and Sprays* **23** (1) 47
[6] Sazhin S S 2014 *Droplets and Sprays* (London, Springer)
[7] Rybdylova O, Osiptsov A N, Sazhin S S, Begg S and Heikal M 2016 *International J of Heat and Fluid Flow* **58** 93
[8] Goldfarb I, Goldshtein V, Kuzmenko G, and Sazhin S S 1999 *Combustion Theory and Modelling* **3** 769